Fluid Simulation of Large Tokamak Plasmas Using a Variable Spatial Mesh, Variable Time Step Implicit Procedure

W.A. Houlberg and R.W. Conn

March 1977

UWFDM-201

Presented at the Mathematics and Computations Division ANS Topical Meeting, Tucson, Arizona, March 28-30, 1977.

FUSION TECHNOLOGY INSTITUTE

UNIVERSITY OF WISCONSIN

MADISON WISCONSIN

Fluid Simulation of Large Tokamak Plasmas Using a Variable Spatial Mesh, Variable Time Step Implicit Procedure

W.A. Houlberg and R.W. Conn

Fusion Technology Institute
University of Wisconsin
1500 Engineering Drive
Madison, WI 53706

http://fti.neep.wisc.edu

March 1977

UWFDM-201

Presented at the Mathematics and Computations Division ANS Topical Meeting, Tucson, Arizona, March 28-30, 1977.

UWFDM-201

Fluid Simulation of Large Tokamak Plasmas Using a Variable Spatial Mesh, Variable Time Step Implicit Procedure

Wayne A. Houlberg
Robert W. Conn

March 1977

Fusion Technology Program
Nuclear Engineering Department
University of Wisconsin
Madison, Wisconsin 53706

Presented at the American Nuclear Society Mathematics and Computations Division Topical Meeting, March 28-30, 1977, in Tucson, Arizona. Also to be published in Nuclear Science and Engineering, September 1977.

ABSTRACT

Research on the development of numerical techniques to simulate the space-time evolution of large tokamak plasmas is reported. A non-uniform spatial mesh technique is employed to allow more accurate calculations in the boundary of reactor size plasmas. A box integration method is used to maintain the accuracy of central differencing on the non-uniform spatial mesh and to preserve both the particle and energy flux. A variable implicit technique is used for the time expansion. The time-centered (Crank-Nicholson) technique used in most other models generally offers greater accuracy but can lead to severe limitations on the time step. Somewhat more implicit treatments can remove the numerical limitations on the timestep without seriously affecting accuracy. The physical time scales, which can change by several orders of magnitude from startup to equilibrium, can then be used to continually adjust the timestep throughout a calculation. Sample calculations are presented for a near-term tokamak engineering test reactor (TETR) and a conceptual tokamak power reactor, UWMAK-III.

I. Introduction

A tokamak is an axially symmetric toroidal device in which the hot plasma is contained by a combination of a strong toroidal magnetic field and a weaker poloidal magnetic field (Figure 1). The poloidal field is produced by driving a toroidal current in the plasma which acts as the secondary of a transformer. The resulting magnetic field lines have a helical shape and generate a set of nested magnetic flux surfaces. Particle and energy flow on a magnetic surface is very rapid since the transport processes are not impeded by the magnetic field. Transport from one magnetic surface to another is responsible for removing particles and energy from the system on a much larger time scale.

From magnetohydrodynamic stability analyses, tokamaks have generally been considered to be limited to low values of β ($\lesssim 5\%$) where β is the ratio of the plasma pressure to the magnetic field pressure. The flux surfaces are nearly concentric with this approximation. Higher values of β may be allowed if the plasma is elongated vertically or if broader toroidal current profiles can be frozen into the plasma during startup. One dimensional plasma transport codes treat the plasma as a cylinder uniform in the azimuthal and poloidal coordinates.[1] The spatial variation is in the radial coordinate measured from the minor axis of the plasma. Vertically elongated plasmas are generally treated as equivalent circles with geometric effects incorporated into the cross-field transport coefficients.

The basic particle and energy transport equations are found by taking moments of the kinetic equation. When a Fokker-Planck collision operator is used with the toroidal geometry of a tokamak, a "neoclassical"

model for plasma transport is found.[2] Averages over a magnetic flux surface yield a set of fluid equations with one dimensional spatial variation. The fluids are electrons, ions, and other ionic species with Maxwellian distributions in velocity space giving characteristic temperatures for each fluid. In addition, Maxwell's equations can be added to relate the toroidal current profile and the poloidal magnetic field to the plasma electrical conductivity. This set of equations is more important for a plasma which depends primarily on ohmic heating than a large ignited neutral beam driven device. A fixed toroidal current profile is used here since it does not greatly affect the analysis.

Microinstabilities and the resulting turbulence are expected to dominate over collisional processes in governing the transport in tokamaks.[3] For these processes, a certain amount of empirical modeling is needed for the energy and particle transport coefficients because of their large uncertainty. The one dimensional particle and energy fluid transport equations are of the general form:

$$\frac{\partial n_i}{\partial t} = \frac{1}{r}\frac{\partial}{\partial r}(r\Gamma_i) - \frac{n_i^2 \langle\sigma v\rangle_{DT}}{2} + S_p\,(r,t) \tag{1}$$

$$\frac{\partial}{\partial t}\left(\frac{3}{2} n_e k T_e\right) = \frac{n_i^2 \langle\sigma v\rangle_{DT}}{4} E_\alpha U_{\alpha e} + \frac{1}{r}\frac{\partial}{\partial r}\left[r\left(Q_e + \frac{3}{2} k T_e \Gamma_e\right)\right]$$

$$- Q_{ei} - P_{rad} + P_{ohm} + P^e_{INJ} \tag{2}$$

$$\frac{\partial}{\partial t}\left(\frac{3}{2} n_i k T_i\right) = \frac{n_i^2 \langle\sigma v\rangle_{DT}}{4} E_\alpha U_{\alpha i} + \frac{1}{r}\frac{\partial}{\partial r}\left[r\left(Q_i + \frac{3}{2} k T_i \Gamma_i\right)\right]$$

$$+ Q_{ei} + P^i_{INJ} - P_{cx} \tag{3}$$

where:

n_e, n_i = electron and ion densities

T_e, T_i = electron and ion temperatures

$U_{\alpha e}$, $U_{\alpha i}$ = fraction of alpha energy to electrons and ions

Q_{ei} = electron-ion rethermalization term

P_{rad} = bremsstrahlung, line, recombination and synchrotron radiation losses

P_{ohm} = ohmic heating

P^e_{INJ}, P^i_{INJ} = electron and ion heating sources from neutral beam injection and/or rf

P_{cx} = charge exchange energy loss

$S_p(r,t)$ = particle source due to neutral beam injection, pellets and ionization of neutrals

Γ_e, Γ_i = electron and ion particle fluxes

Q_e, Q_i = electron and ion energy conduction terms

The particle and heat flow terms can be expressed in terms of a general set of heat and particle transport coefficients as:

$$\Gamma_j = D_{jn} \frac{\partial n}{\partial r} + D_{je} \frac{\partial T_e}{\partial r} + D_{ji} \frac{\partial T_i}{\partial r} \tag{4}$$

$$Q_j = \chi_{jn} \frac{\partial n}{\partial r} + \chi_{je} \frac{\partial T_e}{\partial r} + \chi_{ji} \frac{\partial T_i}{r} \tag{5}$$

The full set of transport coefficients (D,χ) can be incorporated for "neoclassical" modeling.[2] Transport coefficients for microinstabilities are less well known and a "diagonal" model for particle and energy transport is typically used. Transport coefficients for the trapped particle micro-instabilities are used in the calculations in this paper with the diagonal model:

$$\Gamma_i = D_i \frac{\partial n_i}{\partial r} \tag{6}$$

$$Q_{e,i} = \chi_{e,i} \frac{\partial(kT_{e,i})}{\partial r} \qquad (7)$$

The coefficients D_i, χ_e and χ_i are basically the same as those given by Rutherford and Düchs[4] and consist of a summation over several transport processes which are functions of electron and ion temperatures and densities and the temperature and density gradients. Additional particle and energy balance equations can be added to the above set to consider thermal components of the alpha particles or other impurities. The electron density and particle flux are then found from the ionic terms by requiring charge neutrality:

$$n_e = \sum_j Z_j n_j \qquad \text{all ionic species}$$

$$\Gamma_e = \sum_j Z_j \Gamma_j \qquad \text{all ionic species}$$

For a more detailed discussion of the transport equations and the methods used by various transport codes, see the paper by J. Hogan.[1]

The energy source terms from externally injected neutral beams and fusion alphas (3.52 MeV) are found by solving the problem of a high energy ion thermalizing on a background fluid of ions and electrons. Instantaneous thermalization is generally assumed if the thermalization time is short compared to the characteristic time variation of the densities and temperatures. Finite thermalization times for high energy alphas are included in our model as an option to investigate the effects on dynamic behavior but the numerical results presented here do not incorporate that option. The thermal components of the alpha particles are also neglected here to simplify the discussion of the basic numerical treatments.

A fine radial mesh is generally required in the boundary region for two potentially very important problems: (1) sharp density gradients due to action of a poloidal divertor[5,6] and (2) short penetration depths of cold neutrals and impurities entering the plasma from the chamber walls. Strong parallel loss terms along the field lines in the divertor region between the plasma surface and the wall can lead to sharp density gradients of a few centimeters at the plasma boundary.[7] Cold neutrals at the plasma edge can typically have mean free paths of the order of one centimeter. In both cases, a fine radial mesh is required for a reasonably accurate numerical treatment of the physical models. Uniform spatial mesh treatments are able to handle the fine mesh requirements in simulation of currently operating tokamaks. However, a large tokamak with a minor radius of 2-4 meters would require an inordinately large number of radial mesh points for a uniform fine mesh and would consume more computer time and storage than is justifiable.

In this paper we present the development of numerical techniques especially suited for solving the above set of fluid transport equations applied to large tokamak plasmas. A non-uniform spatial mesh is employed (Section II) to allow for fine mesh treatments in the boundary region of a reactor size plasma while a coarser mesh is used in the central plasma region. A box integration method is used to maintain the accuracy of central differencing on the non-uniform grid while conserving both the particle and energy fluxes. A variable implicit technique is used for the time mesh treatment (Section III). The accuracy of a central

differenced (Crank-Nicholson) technique can sometimes be offset by severe limitations in the time step with associated increases in calculation time. More implicit treatment can then be used to eliminate the numerical limitations on the time step without seriously affecting the time history. The time scales for physical processes, which can change by several orders of magnitude from start up to equilibrium, are used to continually adjust the time step size. These techniques have been employed in a computer program which has evolved from an early version of the Oak Ridge Code.[1]

II. Spatial Mesh Finite Difference Treatment

The basic set of transport equations consist of the three nonlinear coupled parabolic partial differential equations given in Equations 1-3. A box integration method is employed to obtain a set of finite difference equations in space for a non-uniform spatial grid.[8] The equations are integrated over a cylindrical shell from $r - \Delta r_-/2$ to $r + \Delta r_+/2$ (see Figure 2) where Δr_+ and Δr_- designate the mesh size between points i, i+1 and i, i-1, respectively. The finite difference expressions for the diffusion terms then become:

$$\frac{1}{r}\frac{\partial}{\partial r}(r\Gamma)\bigg|_i = \frac{1}{I_v}\int_{r-\Delta r_-/2}^{r+\Delta r_+/2}\frac{1}{r}\frac{\partial}{\partial r}(r\Gamma)r\,dr = \frac{1}{I_v}(\Gamma^{i+1/2} - \Gamma^{i-1/2}) \tag{8}$$

where $I_v = \int_{r-\Delta r_-/2}^{r+\Delta r_+/2} r\,dr$

$$\Gamma^{i\pm1/2} = \Gamma\Big|_{r\pm\frac{\Delta r_\pm}{2}} = D^{i\pm1/2}\left.\frac{\partial n}{\partial r}\right|_{i\pm1/2} \tag{9}$$

$$\left.\frac{\partial n}{\partial r}\right|_{i\pm1/2} = \pm\frac{n_{i\pm1} - n_i}{\Delta r_\pm} \tag{10}$$

The energy flow terms are treated in the same manner.

Inside the plasma, the transport coefficients are expected to be continuous functions of radius but possibly have strong radial variation. In this case, the transport coefficients are evaluated as:

$$D^{i\pm1/2} = \frac{D^{i} + D^{i\pm1}}{2} \tag{11}$$

If a step change in the radial transport coefficents is anticipated across the boundary between the plasma and the divertor zone, they can be evaluated at the first mesh point inside each zone:

$$D^{N\pm1/2} = D^{N\pm1} \tag{12}$$

This differencing method preserves the accuracy of central differencing even for the non-uniform mesh. It also conserves the particle and heat fluxes since the differenced expression for the flux leaving region i is the same as the expression for the flux entering region i + 1.

The non-diffusive terms (volumetric source and loss terms) are assumed to be constant over the differential region at values given at each mesh point. The accuracy of this approximation is reduced when a non-uniform mesh is used. Small variations in mesh size from region to region can reduce the error. The alternative is to include a linear variation in the terms through the region by incorporating the values at $i \pm 1$ into the volume averaged term at i.

The boundary conditions at the center are that the fluxes vanish:

$$\Gamma,\ Q_e,\ Q_i \Big|_{r\,=\,0} = 0 \tag{13}$$

At the plasma edge, boundary conditions on the ion density and electron and ion temperatures are of the form

$$\alpha n + \beta \frac{\partial n}{\partial r} = \gamma$$

with the usual choices of

$$\beta = 0 \quad : n\big|_a = n(a) \tag{14a}$$

$$\text{or} \quad \gamma = 0 \quad : \frac{1}{n}\frac{\partial n}{\partial r}\bigg|_a = -\frac{1}{\Delta_n} \tag{14b}$$

where a is the plasma minor radius. The expression in (14b) is the form used for both temperatures and density in the calculations presented here.

The transport coefficients for the trapped particle microinstabilities[3] are functions of the density and temperature gradients through their dependence on the diamagnetic drift frequency and the temperature drift frequency. For simulation of both near term and large power producing Tokamak plasmas such as the Tokamak Engineering Test Reactor (TETR)[9] and UWMAK-III,[10] this leads to oscillations when the mesh size is less than about 5% of the plasma radius and central differencing is used for the gradient dependence of the transport coefficients. The oscillations are primarily due to the $(1/n \cdot \partial n/\partial r)^2$ dependence of the dissipative trapped ion mode which dominates the transport. To eliminate this problem, the density and temperature are fitted by least squares to a power series at each timestep in the same manner as is done in the Princeton code.[4]

$$\ln\left(\frac{n}{n_o}\right) = \sum_{j=1}^{J} C_{nj}\left(\frac{r}{a}\right)^{2(j-1)} \tag{15}$$

The logarithmic derivatives of density and temperature are then evaluated from the fitted profiles.

$$\frac{1}{n}\frac{\partial n}{\partial r} = \sum_{j=2}^{J} 2(j-1)\, C_{nj}\left(\frac{r}{a}\right)^{2j-3}\frac{1}{a} \tag{16}$$

The order of the fit can be specified in the range $2 < J < 10$. For $J = 1$, a central difference is used for the gradients.

The effects of various spatial mesh treatments can be discussed independently of the time treatment by examining equilibrium profiles. To illustrate typical numerical results, we present sample calculations for two types of large tokamaks. The Tokamak Engineering Test Reactor (TETR)[9] is a conceptual design of an unignited neutral beam driven device utilizing the two component operating mode[11] potentially capable of producing a high neutron wall loading for materials and blanket engineering tests. UWMAK-III[10] is a conceptual design for a power producing (2000 MW_e) tokamak. Tables I and II summarize the basic parameters for simplified physical models of TETR and UWMAK-III respectively. Boundary conditions are chosen to be consistent with anticipated characteristic gradients under the action of a poloidal divertor.[7]

Typical equilibrium profiles for the ion density and electron and ion temperatures are given in Figure 3 for TETR and Figure 4 for UWMAK-III. In both cases, the density decreases by more than two orders of magnitude from the center of the plasma to the edge. The addition of a neutral gas recycling model would produce flatter density profiles typical in currently operating tokamaks. The temperature profiles are fairly flat in both cases with edge temperatures in the several keV range. Neutral gas recycle and radiation cooling effects of impurities lower the edge temperatures when these models are included. Figure 5 shows the typical radial variation of the electron heat conduction coefficient for the TETR calculations. The dominant transport mechanism in each region is indicated. The ion heat conduction coefficient, χ_i, and the particle diffusion coefficient, D, have similar profiles. The transport coefficients in the UWMAK-III calculations are the same order of

magnitude with similar radial profiles.

Various spatial meshes have been tested with TETR and UWMAK-III parameters. Sensitivity to the order of the gradient fit, J, for the transport coefficients has also been examined. The most important question of accuracy of the gradient fitting is whether the trapped particle modes are sensitive to local values of the gradients and if so, how much physics is lost in smoothing the gradient dependence.

The central values of density and temperature are virtually unaffected by the various mesh sizes and order of gradient fit. The edge values show the greatest variation due to the sharp gradients imposed by the boundary conditions. Tables III and IV show the edge denisty, n(a), converges to about $2.3 \times 10^{12} cm^{-3}$ in TETR and the edge electron temperature, $T_e(a)$ to about 3.3 keV for all values of J and all sizes of edge mesh less than 2 cm. Relatively few mesh points (41) are required for an accurate uniform mesh treatment of this model.

Tables V and VI show the variation of n(a) and $T_e(a)$ for the UWMAK-III model for several mesh sizes and values of J. n(a) generally decreases and $T_e(a)$ increases as the mesh size is decreased and J is increased. The finest uniform mesh case (N = 97) has a 4 cm mesh. The non-uniform mesh case (N=48) employs a 2 cm mesh over the outer 40 cm of plasma radius and gives 10% higher temperatures at r=a than the finest uniform mesh case. Thus, as expected, the variable radial mesh treatment is more important for UWMAK-III size plasmas than for TETR parameters. A finer mesh treatment would be even more critical when divertor and neutral gas recycle models are included.

III. Time Mesh Treatment

The time dependence of the particle and energy balance equations is treated implicitly by expanding each term in time about $t + \theta\Delta t$. Only the first order terms in Δt are kept which leads to a linearized set of equations in density and temperature at the new time. For $\theta = 0$, the equations reduce to the Euler method while $\theta = .5$ is the Crank-Nicholson method and $\theta = 1$ is pure implicit. Let f be an arbitrary term in one of the equations and k be an index denoting the timestep, then:

$$f(n_i, T_e, T_i)\Big|_{t_k+\theta\Delta t_k} = f^k + \theta\{\frac{\partial f^k}{\partial n_i}(n_i^{k+1}-n_i^k) + \frac{\partial f^k}{\partial T_i}(T_i^{k+1} - T_i^k) + \frac{\partial f^k}{\partial T_e}(T_e^{k+1} - T_e^k)\} \qquad (17)$$

The expressions f^k, $\frac{\partial f^k}{\partial n_i}$, $\frac{\partial f^k}{\partial T_e}$ and $\frac{\partial f^k}{\partial T_i}$ are re-evaluated at each timestep.

The transport coefficients are treated explicitly but evaluated at densities and temperatures extrapolated in time with a type of predictor treatment. For example,

$$D(n_i,T_e,T_i)\Big|_{t_k+\theta\Delta t_k} = D(n_i',T_e',T_i') \qquad (18)$$

$$n_i' = n_i^k + \theta\Delta t_k \left.\frac{\partial n_i}{\partial t}\right|^k$$

$$n_i' = n_i^k \left[1 + \theta \frac{\Delta t_k}{\tau_n^k}\right] \qquad (19)$$

$$\tau_n^k = \frac{n_i^k}{\partial n_i/\partial t\Big|_k} = \frac{n_i^k \, \Delta t_{k-1}}{n_i^k - n_i^{k-1}} \tag{20}$$

The characteristic times, τ, are calculated at each timestep for each variable and radial mesh point. A very small timestep is initially taken with all $\tau = 0$ to start the calculation. Subsequent timesteps are then limited to 10% of the shortest characteristic time for density or temperature variation at any radial mesh point up to a specified maximum timestep size as equilibrium is approached. The 10% limit on $\Delta t_k/\tau^k$ puts an upper bound on the variation in the predicted densities and temperatures (Eqn. 19).

Because the equations are linearized at each timestep, a simplified analysis of the numerical treatment can be made. At each timestep, the equations are put into the form

$$\underline{\underline{A}}\ \underline{x}^{k+1} = \underline{\underline{B}}\ \underline{x}^k + \underline{C}$$

where $\underline{x}$ represents the density and temperature spatial arrays and k the timestep index. Numerical stability can be investigated by examining the eigenvalues of the homogeneous equation.[12]

For pure diffusion and conduction with no coupling between the density and temperature equations, it can be shown that all eigenvalues are bounded in the range [-1,1] if $.5 \leq \theta \leq 1$ and no numerical oscillations arise to limit the timestep. Unstable oscillations can occur for $\theta < .5$ if Δt is too large. The Crank-Nicholson method gives the most accurate treatment for linear equations because of the time centered differences.[12] The accuracy for a nonlinear equation is more difficult to assess because of the lack of analytic solutions. The addition of density and temperature dependent sources and coupling between the density and temperature equations can decrease the limits on Δt for which no unstable oscillations

occur. Small radial mesh size coupled with large transport coefficients can reduce the maximum allowable Δt for stability much below the physical time scales for $\theta = .5$ or even somewhat more implicit methods. An optimum choice of θ would be close to .5 to maintain the advantages of time centered difference but large enough to avoid numerical oscillations in a given physical model with an appropriate radial mesh for spatial accuracy.

Calculations have been made on TETR and UWMAK-III parameters to determine the effect of various values of θ on CPU time and the time history of the evolution of the density and temperature profiles. The calculations are initialized with low values of temperature (about 200 eV) typical of the ohmic heating phase in tokamaks. In TETR, the 150 MW of neutral beam power heats the plasma to equilibrium in about 300 msec where a particle confinement time of $\tau_p \sim 35$ msec is found. In the UWMAK-III calculations, 500 MW of injection energy is used for 1.5 sec to heat the plasma to ignition at full density ($7.9 \times 10^{13} cm^{-3}$). Heating by the fusion alphas then brings the plasma to equilibrium at about 5.0 sec where the particle confinement time is about 350 msec.

Table VII shows the effect of various mesh calculations for TETR on the maximum timestep for stability with $\theta = 0.5$ and on the CPU time for $\theta = 0.5$, 0.6 and 1. An upper limit of 1 msec is imposed on the timestep in all cases. For the finest mesh cases (1 cm), the timestep has to be limited to 0.5 msec to avoid numerical oscillations with $\theta = 0.5$. All cases with $\theta = 0.6$ or 1.0 give numerically stable solutions. The variable mesh case coupled with $\theta = 0.6$ or 1.0 give a factor of 4 reduction in CPU time over the fine mesh, $\theta = 0.5$ case.

The savings in CPU time for variable mesh and $\theta > 0.5$ is more pronounced in reactor (UWMAK-III) calculations. Table VIII shows that fine mesh cases with $\theta = 0.5$ leads to a much more severe limitation on the maximum timestep with an associated increase in the CPU time for a typical calculation. An upper limit of 10 msec on the timestep is based on the particle confinement time. All cases with $\theta = 0.6$ and 1.0 give numerically stable solutions with reductions in CPU time up to an order of magnitude over the variable mesh case with $\theta = 0.5$.

For all TETR and UWMAK-III calculations, no significant differences were noted in the time histories of the temperature and density profiles using $\theta = 0.5$, 0.6 and 1.0. The equilibrium reached is independent of θ. If the effects of various physical models on equilibrium profiles only are of primary interest, fully implicit calculations can be used to avoid any numerical oscillations.

IV. Summary and Conclusions

We have developed a series of techniques for computer simulation of large tokamaks which yield very stable numerical solutions to one-dimensional transport problems. The basic solving techniques make efficient use of computer time which is especially important when one desires to carry out parametric studies which typically require many computer runs. The fine mesh treatment allows a better analysis of the important region between the plasma and the chamber wall. A slab model for neutrals which includes reflection of neutrals at the wall and sputtering of wall material has been included in the computer program. The divertor model of Mense[7] is incorporated to permit more thorough parameter studies.

Improved models for line and recombination radiation for various high Z impurities have recently been added based on experimental measurements. An improved model for synchrotron radiation is being studied. Work is continuing on an RF heating package to evaluate various techniques for heating the plasma to ignition. Other aspects of tokamak modeling already added to the basic fluid treatment are: a pencil beam model including beam/plasma fusions, an alpha particle transport model, and finite thermalization time of the fusion alphas. Overall, the resulting mathematical model is flexible enough to study a wide range of important physical processes anticipated for large tokamak plasmas.

Acknowledgements

The authors would like to thank Dr. J. T. Hogan for originally making an early version of the Oak Ridge Tokamak transport code available. This research was supported under grants from the Energy Research and Development Administration and the Wisconsin Electric Utilities Research Foundation.

References

1. J. T. Hogan, "Multifluid Tokamak Transport Models", in Methods in Computational Physics, ed. by J. Killeen, B. Alder, S. Fernback and M. Rotenberg, Academic Press (1976), Vol. 16, p. 131.

2. F. L. Hinton and R. D. Hazeltine, Reviews of Modern Physics 48, 239 (1976).

3. For the trapped ion mode see M. N. Rosenbluth, D. W. Ross and D. P. Kostomarov, Nucl. Fusion 12, 3 (1972). For the trapped electron mode see J. C. Adam, W. M. Tang and P. H. Rutherford, Phys. Fluids 19, 561 (1976).

4. P. H. Rutherford and D. F. Duchs, "A Computer Model of Radial Transport in Tokamaks", MATT-1272, Princeton Plasma Physics Laboratory (1976).

5. G. A. Emmert, A. T. Mense and J. M. Donhowe, Proc. 1st Topical Meeting on Technology of Controlled Thermonuclear Fusion, San Diego, (April 1974).

6. A. T. Mense, G. A. Emmert, and J. D. Callen, Nuclear Fusion 15, 703 (1975).

7. A. T. Mense, Ph.D. Thesis, Univ. of Wisconsin, Madison (1977).

8. E. L. Washspress, Iterative Solution of Elliptic Systems, Prentice-Hall Englewood Cliffs, New Jersey (1966).

9. R. W. Conn and D. L. Jassby, "A Tokamak Engineering Test Reactor", published in Proc. Int'l. Conf. on Radiation Test Facilities for the CTR Surface and Materials Program, ANL/CTR-75-4, Argonne National Laboratory (1975). G. L. Kulcinski, R. W. Conn, C. W. Maynard, et al., "TETR - A Tokamak Engineering Test Reactor . . .", to be published in the Proc. of the 2nd ANS Topical Meeting on the Technology of Controlled Nuclear Fusion, Richland, Washington, (Sept. 21-23, 1976).

10. R. W. Conn, G. L. Kulcinski, C. W. Maynard, et al., "A High Performance Noncircular Tokamak Power Reactor Design Study - UWMAK-III", to be published in Proc. of the Sixth IAEA Conf. on Plasma Physics and Controlled Nuclear Fusion Research, Berchtesgaden, West Germany (Oct. 6-13, 1976).

11. J. M. Dawson, H. P. Furth and F. H. Tenney, Phys. Rev. Lett. 26, 1156 (1971).

12. For examples of this treatment see G. E. Myers, Analytical Methods in Conduction Heat Transfer, McGraw-Hill (1971).

FIGURE TITLES

FIGURE 1: Schematic diagram of the major components of a tokamak with the helical path of a magnetic field line indicated in the lower portion of the figure. (Figure courtesy of PPPL).

FIGURE 2: Non uniform radial mesh at grid point i and radius r indicating the radial region associated with grid point i in the box integration $(r - \Delta r_- /2, r + \Delta r_+ /2)$.

FIGURE 3: Typical equilibrium radial profiles of ion density and electron and ion temperatures in TETR test case.

FIGURE 4: Typical equilibrium radial profiles of ion density and electron and ion temperatures in UWMAK-III test case.

FIGURE 5: Typical equilibrium radial profile of the electron heat conduction coefficient in TETR test case with the dominant transport term indicated in each radial region.

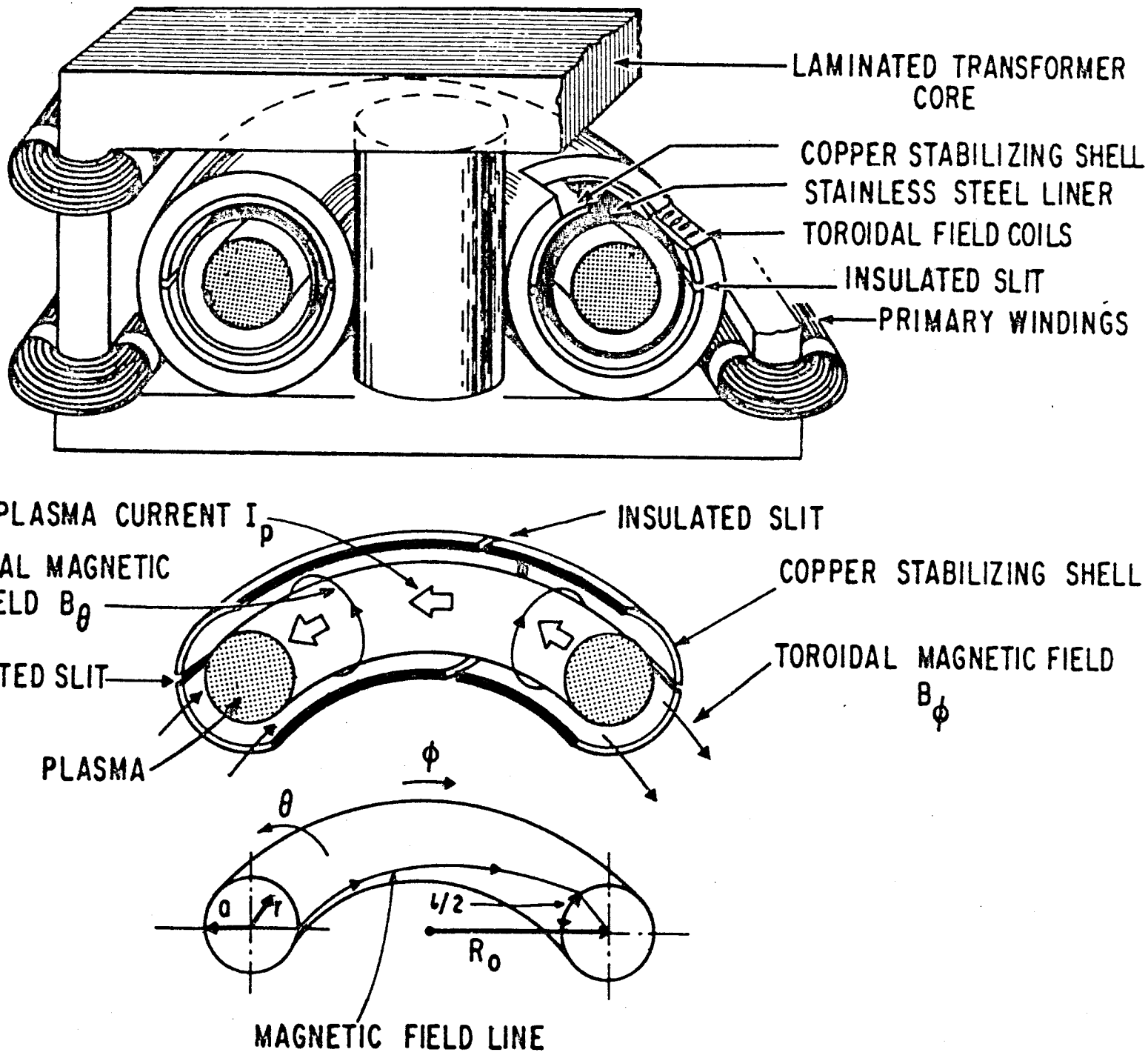
LAMINATED TRANSFORMER CORE
COPPER STABILIZING SHELL
STAINLESS STEEL LINER
TOROIDAL FIELD COILS
INSULATED SLIT
PRIMARY WINDINGS
PLASMA CURRENT I_p
INSULATED SLIT
POLOIDAL MAGNETIC FIELD B_θ
COPPER STABILIZING SHELL
INSULATED SLIT
TOROIDAL MAGNETIC FIELD B_ϕ
PLASMA
ϕ
θ
a
r
L/2
R_0
MAGNETIC FIELD LINE

FIGURE 1

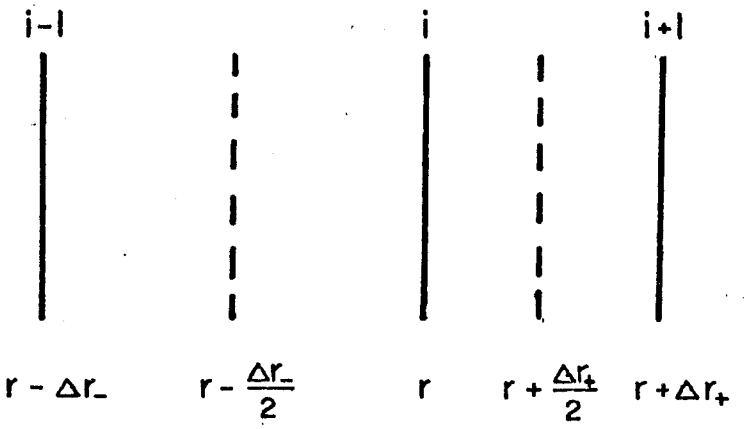

FIGURE 2

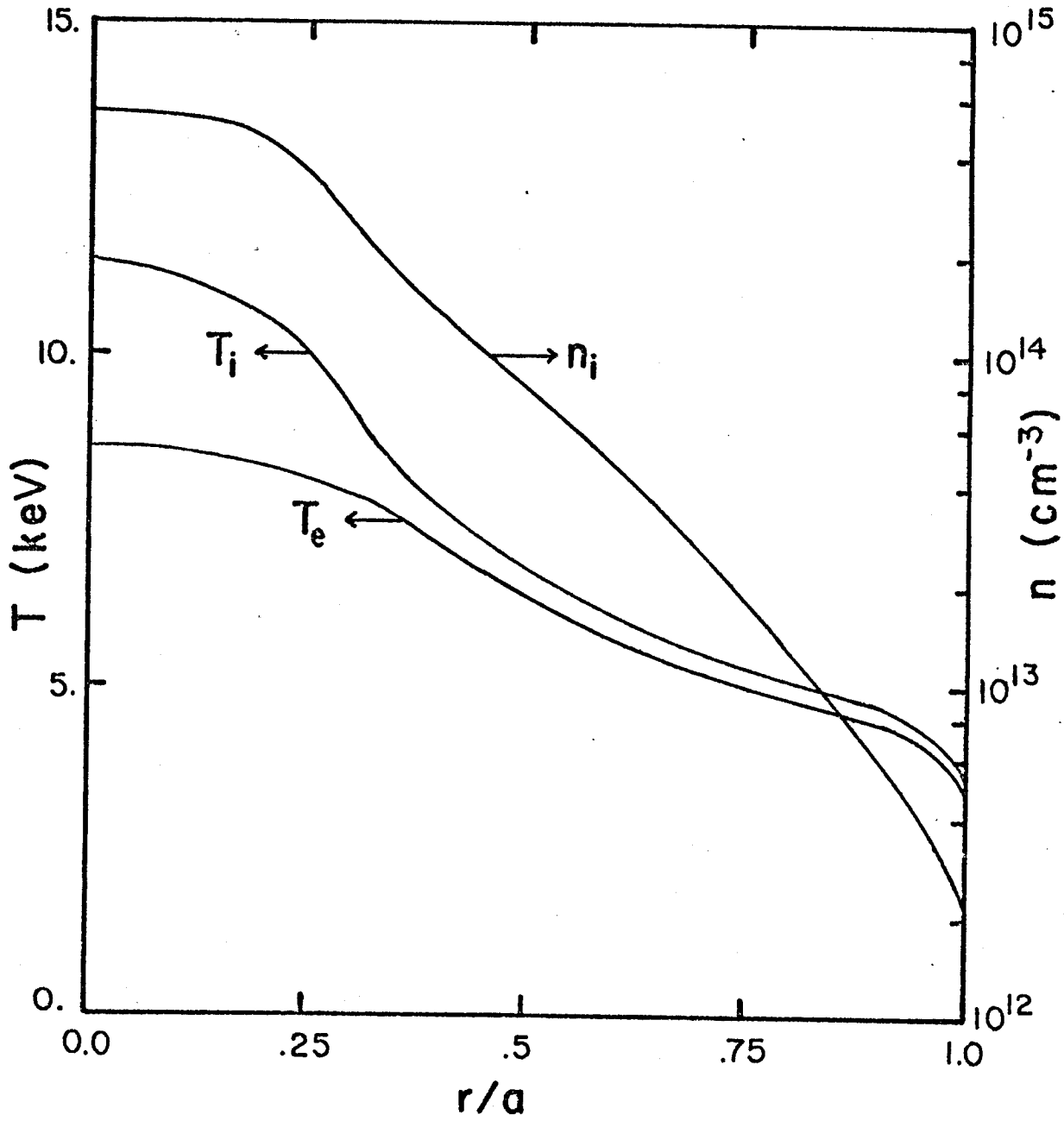

FIGURE 3

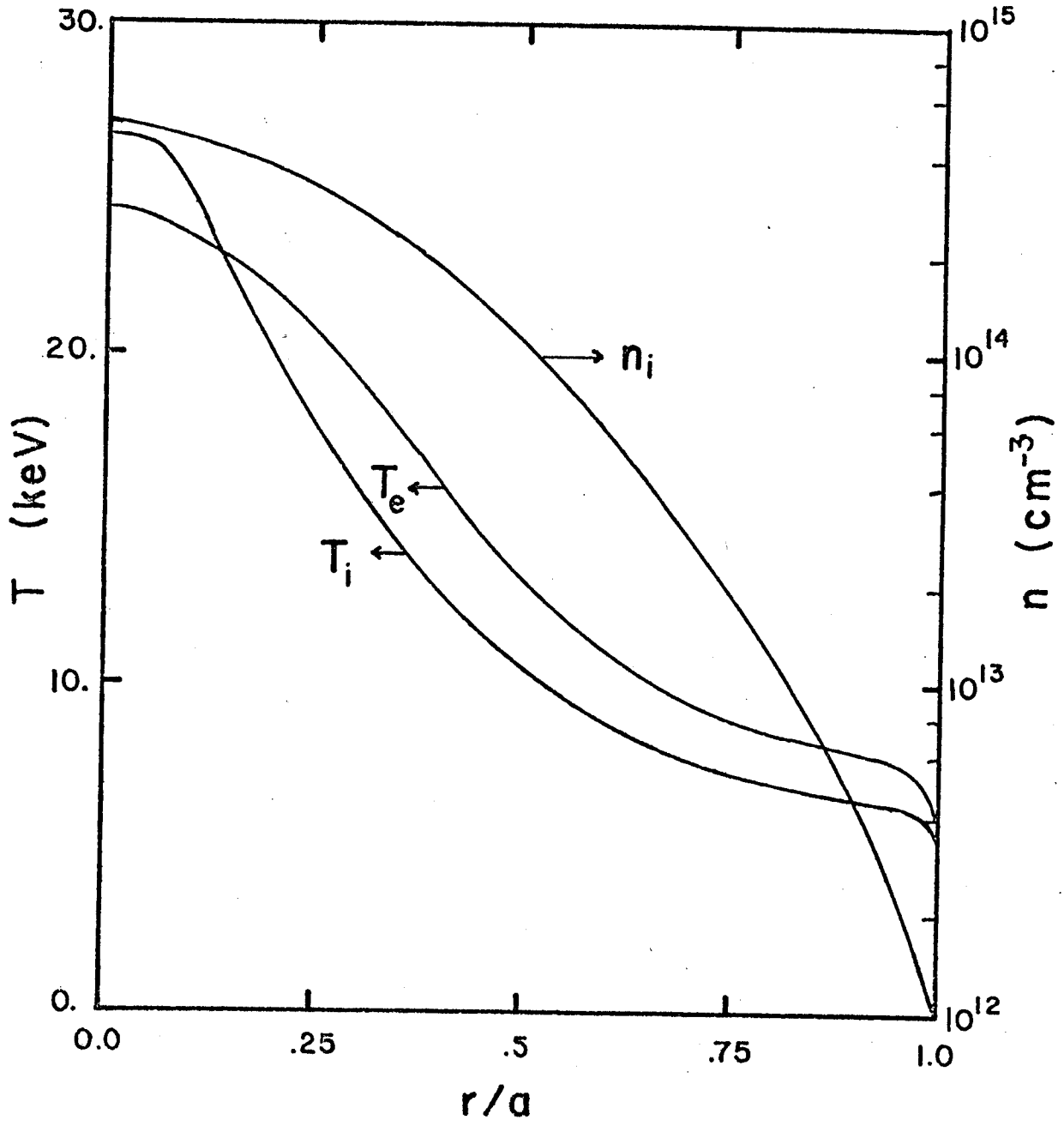

FIGURE 4

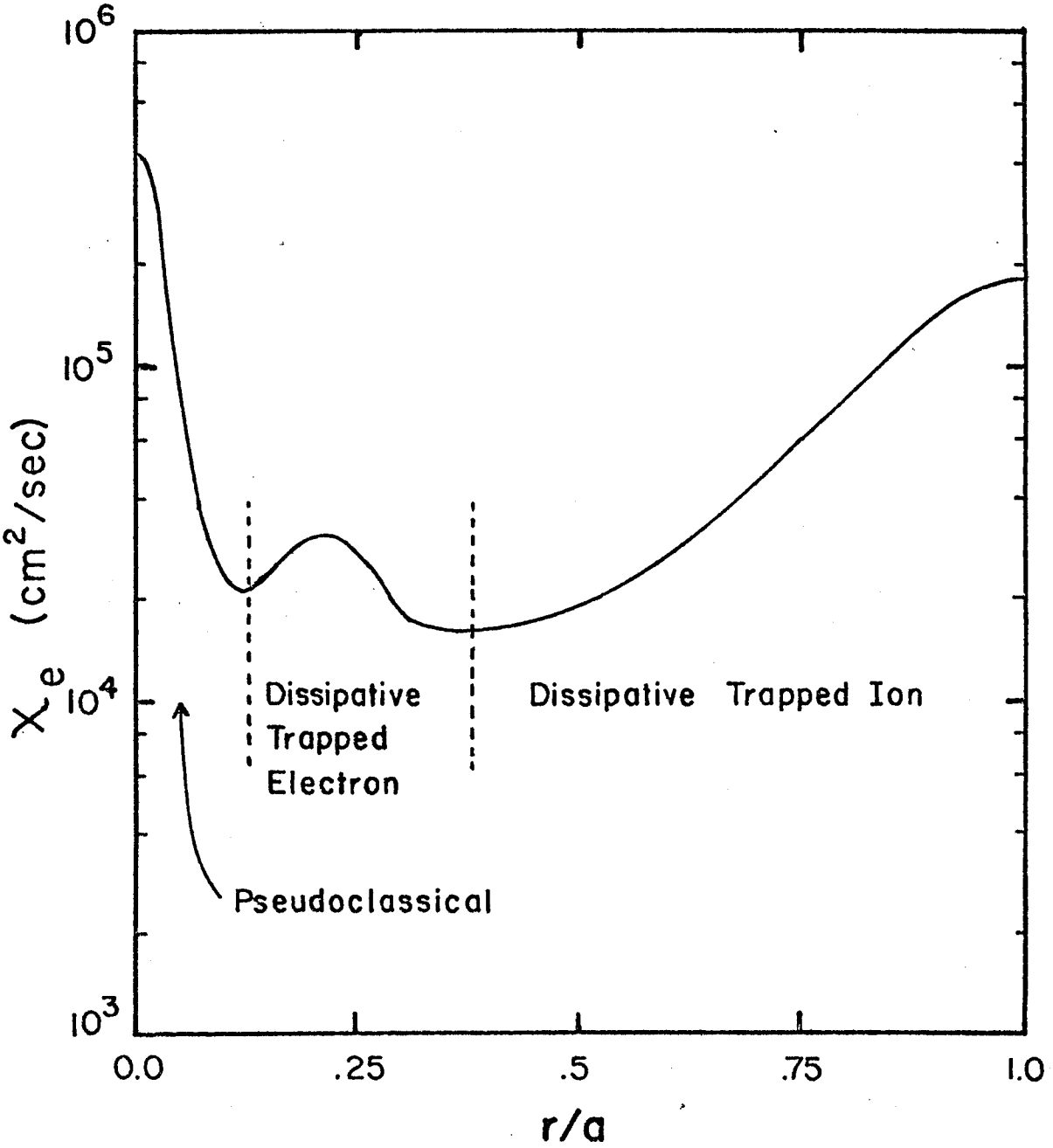
10^6
10^5
10^4
10^3
χ_e (cm^2/sec)
Dissipative
Trapped
Electron
Dissipative Trapped Ion
Pseudoclassical
0.0
.25
.5
.75
1.0
r/a

FIGURE 5

Table I

Parameters for TETR

B_ϕ = 4.19 T - toroidal magnetic field on plasma axis

R_o = 3.24 m - major radius of torus

a = .60 m - minor radius of plasma in midplane

a_{eff} = .80 m - effective minor radius for circular plasma

I_ϕ = 2.52 x 10^6 A - toroidal plasma current

E_o = 150 keV - deuterium beam injection energy

P_B = 150 MW - injected neutral beam power

Boundary conditions at plasma surface:

Δ_n = .05 m

Δ_{T_e} = .10 m

Δ_{T_i} = .10 m

Physical Model:

No neutral gas recycle, impurities or thermal alphas

Instantaneous thermalization of fusion alphas

Dissipative trapped particle model for transport coefficients

Table II

Parameters for UWMAK-III

B_ϕ = 4.05 T - toroidal magnetic field on plasma axis

R_o = 8.10 m - major radius of torus

a = 2.70 m - minor radius of plasma in midplane

a_{eff} = 3.84 m - effective minor radius for circular plasma

I_ϕ = 15.8 x 10^6 A - toroidal plasma current

Boundary conditions at plasma surface:

Δ_n = .10 m

Δ_{T_e} = .20 m

Δ_{T_i} = .50 m

Physical Model:

No neutral gas recycle, impurities or thermal alphas

Instantaneous thermalization of fusion alphas

Dissipative trapped particle model for transport coefficients

Table III

Plasma Density at the Plasma Edge (cm^{-3}) for TETR for Various Spatial Meshes (N) and Order of Least Squares Fitting (J) to Gradients in Transport Coefficients.

N \ J	3	5	7	Central Difference
11[a]	2.9×10^{12}	2.8×10^{12}	-	4.2×10^{12}
21[a]	2.5×10^{12}	2.4×10^{12}	2.4×10^{12}	2.7×10^{12}
41[a]	2.3×10^{12}	2.3×10^{12}	2.4×10^{12}	(c)
81[a]	2.2×10^{12}	2.3×10^{12}	2.4×10^{12}	(c)
35[b]	2.3×10^{12}	2.2×10^{12}	2.3×10^{12}	-

(a) uniform spatial mesh

(b) nonuniform spatial mesh decreasing to 1 cm at plasma edge

(c) numerically unstable

Table IV

Electron Temperature at Plasma Edge (keV) for TETR for Various Spatial Meshes (N) and Order of Least Squares Fitting (J) to Gradients in Transport Coefficients.

N \ J	3	5	7	Central Difference
11[a]	2.5	2.5	-	2.6
21[a]	2.9	2.9	2.9	2.9
41[a]	3.2	3.2	3.2	(c)
81[a]	3.3	3.3	3.4	(c)
35[b]	3.3	3.3	3.3	-

(a) uniform spatial mesh

(b) nonuniform spatial mesh decreasing to 1 cm at plasma edge

(c) numerically unstable

Table V

Plasma Density at the Plasma Edge (cm^{-3}) for UWMAK-III for Various Spatial Meshes (N) and Order of Least Squares Fitting (J) to Gradients in Transport Coefficients.

N \ J	3	5	7	Central Difference
17[a]	1.06×10^{12}	$.90 \times 10^{12}$	$.89 \times 10^{12}$	1.22×10^{12}
33[a]	1.04×10^{12}	$.82 \times 10^{12}$	$.79 \times 10^{12}$	(c)
49[a]	1.04×10^{12}	$.81 \times 10^{12}$	$.76 \times 10^{12}$	(c)
65[a]	1.05×10^{12}	$.80 \times 10^{12}$	$.75 \times 10^{12}$	(c)
97[a]	1.03×10^{12}	$.78 \times 10^{12}$	$.72 \times 10^{12}$	(c)
48[b]	$.95 \times 10^{12}$	$.78 \times 10^{12}$	$.73 \times 10^{12}$	-

(a) uniform spatial mesh

(b) nonuniform spatial mesh decreasing to 2 cm at plasma esge

(c) numerically unstable

Table VI

Electron Temperature at the Plasma Edge (keV) for UWMAK-III for Various Spatial Meshes (N) and Order of Least Squares Fitting (J) to Gradients in Transport Coefficients.

N \ J	3	5	7	Central Difference
17[a]	3.50	3.56	3.58	3.67
33[a]	4.46	4.49	4.51	(c)
49[a]	4.92	4.93	4.94	(c)
65[a]	5.19	5.18	5.20	(c)
97[a]	5.41	5.39	5.40	(c)
48[b]	5.76	5.81	5.83	-

(a) uniform spatial mesh

(b) nonuniform spatial mesh decreasing to 2 cm at plasma edge

(c) numerically unstable

Table VII

Spatial Mesh at the Plasma Edge, Maximum Timestep for θ = .5 and Computer Time for Sample Runs with θ = .5, .6 and 1 vs. Various Spatial Meshes for a 400 msec TETR Calculation

N Spatial Mesh Points	min Δr (cm)	Δt_{max} (sec) θ=.5	CPU Time (min.)[a] θ=.5	θ=.6	θ=1
11[b]	8	1[d]	.12	.12	.12
21[b]	4	1[d]	.21	.21	.21
41[b]	2	1[d]	.41	.41	.41
81[b]	1	.5[e]	1.37	.90	.86
35[c]	1	.5[e]	.56	.37	.35

(a) for runs on the MFE CDC7600 computer system

(b) uniform spatial mesh

(c) nonuniform spatial mesh decreasing to plasma edge

(d) Δt limited by physical time scale $.5 < \theta < 1$

(e) Δt limited by onset of numerical oscillations for θ = .5

Table VIII

Spatial Mesh at the Plasma Edge, Maximum Timestep for θ=.5 and Computer Time for Sample Runs with θ = .5, .6 and 1 vs. Various Spatial Meshes for a 7.5 Second UWMAK-III Calculation.

N Mesh Spatial Points	min Δr (cm)	Δt_{max}(msec) θ=.5	CPU time (min.)[a]		
			θ=.5	θ=.6	θ =1
17[b]	24	10[d]	.26	.26	.26
33[b]	12	10[d]	.49	.49	.49
49[b]	8	5[e]	1.35	.75	.75
65[b]	6	5[e]	2.14	1.02	1.01
97[b]	4	2.5[e]	4.87	1.62	1.57
48[c]	2	1[e]	6.06	.73	.72

(a) for runs on the MFE CDC7600 computer system

(b) uniform spatial mesh

(c) nonuniform spatial mesh decreasing to plasma edge

(d) Δt limited by physical time scales $.5<\theta<1$

(e) Δt limited by onset of numerical oscillations for θ=.5